

Session I - 1.1

PROMINENCE FINE STRUCTURE, DYNAMICS AND SEISMOLOGY

Solar Prominence Fine Structure and Dynamics

Thomas Berger

National Solar Observatory,
P.O. Box 62, Sunspot, NM, 88349 USA
email: tberger@nso.edu

Abstract. We review recent observational and theoretical results on the fine structure and dynamics of solar prominences, beginning with an overview of prominence classifications, the proposal of possible new “funnel prominence” classification, and a discussion of the recent “solar tornado” findings. We then focus on quiescent prominences to review formation, down-flow dynamics, and the “prominence bubble” phenomena. We show new observations of the prominence bubble Rayleigh-Taylor instability triggered by a Kelvin-Helmholtz shear flow instability occurring along the bubble boundary. Finally we review recent studies on plasma composition of bubbles, emphasizing that differential emission measure (DEM) analysis offers a more quantitative analysis than photometric comparisons. In conclusion, we discuss the relation of prominences to coronal magnetic flux ropes, proposing that prominences can be understood as partially ionized condensations of plasma forming the return flow of a general magneto-thermal convection in the corona.

Keywords. Sun: prominences, Sun: filaments, Sun: magnetic fields, Sun: atmospheric motions, Sun: chromosphere, instabilities, Sun: oscillations, Sun: UV radiation

1. Introduction

It is an honor to be asked to review our state of knowledge of prominence fine structure and dynamics at a meeting dedicated to Professor Einar Tandberg-Hanssen. The number of fundamental results in this field that were directly made or influenced by Prof. Tandberg-Hanssen is truly impressive. Since the last edition of his book (Tandberg-Hanssen 1995), and particularly since the recent launches of the *Hinode* Solar Optical Telescope (SOT; Tsuneta *et al.* 2008) and SDO/AIA instruments (Lemen *et al.* 2011), there has been an explosion of results too numerous to cover in this brief review. Thus I will focus on key results from the last several years and in particular on recent findings in quiescent prominences, my own field of expertise. For broader reviews see Labrosse *et al.* (2010) and Mackay *et al.* (2010).

This article, being based on the first talk of the conference, begins by introducing prominences and filaments[†]. Section 2 briefly reviews current definitions of prominences and the distinctive structures and dynamics in various types. We also discuss whether a new type of coronal condensation, thus far called “funnel prominences”, constitutes a real prominence or is perhaps better understood as a unique condensation event more akin to coronal rain. We conclude the discussion with a review of the so-called “tornado” phenomenon and its relation to other prominence structures. Section 3 then focuses on quiescent prominence dynamics, in particular prominence formation, downflow dynamics, and the enigmatic prominence bubble instability. We conclude by proposing the unifying

[†] As usual we use the term “filaments” to refer synonymously to prominences seen on the disk.

hypothesis that prominences can be understood as largely neutral plasma condensations within magnetic flux ropes in the solar corona, with the observed differences in structure and dynamics caused by variations in the magnetic field strength, plasma ionization degree, and height of the flux rope in the atmosphere.

It will be noticed that the theoretical and measured magnetic structure of prominences is not covered in detail in this review. References to “structure” in this review concentrate primarily on plasma morphology and not on magnetic field topology, although the two are of course linked to varying degrees in different prominence types. Bommier *et al.* (1994) summarizes the pioneering efforts to measure quiescent prominence magnetic fields using the Hanle effect at the Pic du Midi observatory through the 1990s, while Casini *et al.* (2003), López Ariste and Casini (2003), Merenda *et al.* (2006), and Schmieder *et al.* (2013) present more recent measurements. Also notably lacking will be details of radiative transfer models; see Gunár (2013), Berlicki *et al.* (2011), Heinzel *et al.* (2008) for recent progress in this sub-field of prominence research. As with any brief review, omission of key papers in the field is inevitable, due only to my own limitations in following the literature and the required brevity of the review, and not to any intentional neglect.

2. What are prominences and filaments?

Since Prof. Tandberg-Hanssen’s book, there has been a narrowing of the definition of “prominence” to include only those structures composed of relatively low-temperature, $\sim 10^4$ K, plasma in the solar corona that are associated with large-scale, $O(10\text{--}100)$ Mm, magnetic polarity inversion lines (PILs) in the photosphere (Engvold 1998). Equivalently, prominences all lie above chromospheric “filament channels” that form in association with PILs in the photosphere (Lites *et al.* 2010; Gaizauskas *et al.* 1997). Thus so-called “surge prominences” are now classified as active region jet phenomena. Similarly “loop prominences” are now recognized as post-flare loop arcades, quite distinct from any prominence or filament structures on the Sun.

In the following sections we employ the common “active region”, “intermediate”, and “quiescent” prominence classifications to delineate basic variations in prominence characteristics. More sophisticated schemes based on PIL topologies can be found, e.g., in Mackay *et al.* (2008). It should also be noted that there are common structural characteristics in all prominence types, e.g., the “barb” structures that are seen as extensions of filaments reaching downwards (Martin 1998), the “spine” regions which comprise the major axis of the structure (particularly evident in long filaments seen on the disk), and the associated characteristic of “chirality” that is observationally related to the direction of barb formation relative to the PIL (Martin *et al.* 2008).

2.1. Active region prominences

Active region (AR) prominences occur adjacent to sunspots, typically over PILs in associated plage regions. The key structures in AR prominences are long thin threads that occur in groups of relatively horizontal “bundles”. The bundles are generally not straight and can exhibit upward or downward curvature. Thread lengths are typically 5–30 Mm with typical thicknesses of 350–650 km in *Hinode*/SOT images (Okamoto *et al.* 2007). Figure 1 shows a typical AR prominence. Note that the prominence is only 2–3 times higher than the chromospheric spicules, i.e. about 15 Mm in maximum height.

AR prominences are highly dynamic with flows along the thread structures on the order of 10 km s^{-1} (Okamoto *et al.* 2007) and perpendicular (possibly erupting) motions up to 70 km s^{-1} (Kucera *et al.* 2003). The thread groups themselves sometimes rise or appear to twist in impulsive events, with plasma continuing to flow along the threads during these

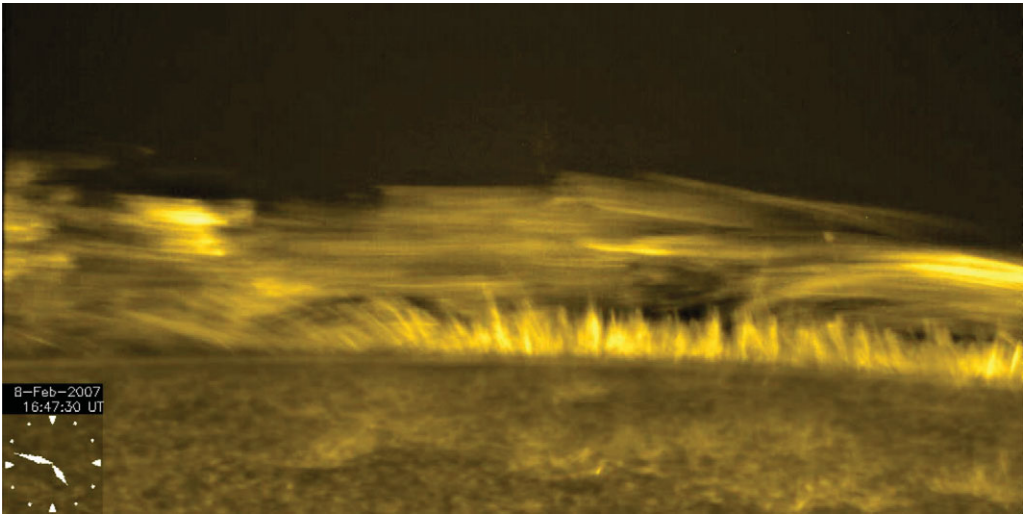


Figure 1. A typical active region prominence seen at the limb in the *Hinode*/SOT Ca II 396.8 nm bandpass on 08-Feb-2007. The image has been rotated to place the solar limb horizontal. Courtesy of J. Okamoto, ISAS/JAXA.

transients. Doppler velocities in AR filaments show only small mostly upward velocities of $\sim 1 \text{ km s}^{-1}$ (Kuckein 2012), perhaps due to localized heating events (Filippov and Koutchmy 2002). AR prominences are the most eruptive of prominences with typical time between eruptions or major “activation” events measured in hours. In comparison, intermediate and quiescent prominence erupt on time scales of days or weeks.

Evidence of Alfvén waves in AR prominences is found with periods of 120–250 s and wavelengths of 250 Mm (Okamoto *et al.* 2007). Prominence oscillation events have been related to pre-eruption dynamics as well (Bocchialini *et al.* 2011). A recent review of prominence “seismology” is given by Ballester (2006).

2.2. Intermediate prominences

Intermediate prominences form outside of active regions, typically in the mid-latitude regions between remnant plage regions that have been sheared by differential rotation to form elongated PILs, sometimes extending for 500 Mm or more. Intermediate prominences do not usually occupy the entire PIL, occurring in shorter segments of order 100 Mm in the extended filament channel.

Like AR prominences, intermediates are composed of a multitude of thin, ~ 300 –500 km, threads. However intermediate prominence threads are shorter in length and occur in upward-arching “dips”, at least when seen at the limb along some sight lines (prominence appearance is highly dependent on the angle of the line-of-sight to the local prominence axis at the limb). Figure 2 shows a typical intermediate prominence at the limb as well as the associated mid-latitude filament. Magnetostatic models of prominences based on extrapolations of measured photospheric magnetic fields appear most similar to intermediate prominences due to their assumption that prominence plasma collects only in concave horizontal dips of the magnetic field (Dudík *et al.* 2008; Aulanier and Demoulin 1998; Aulanier *et al.* 1998; Demoulin *et al.* 1987).

Ahn *et al.* (2010) finds large scale flows with velocities of $\sim 10 \text{ km s}^{-1}$, with evidence of counterstreaming similar to that found in the observations of Zirker *et al.* (1998), in a large intermediate prominence, but more often one observes only localized flows or large scale “rippling” oscillations in these structures. For example, oscillations have been

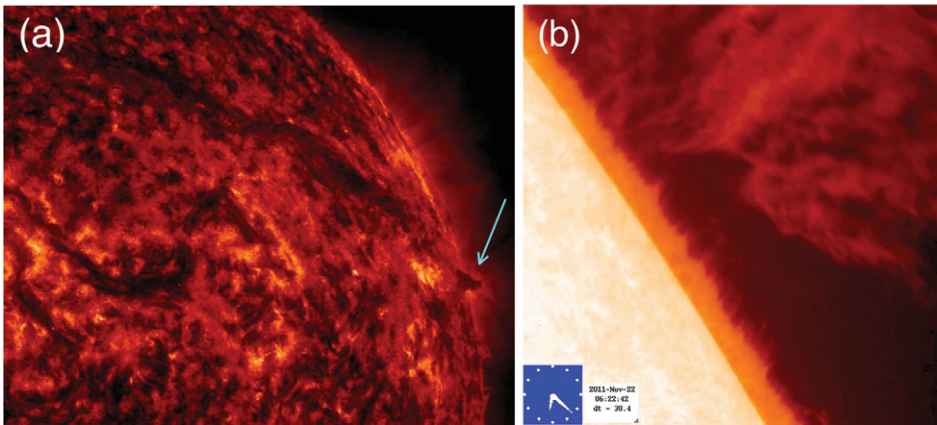


Figure 2. (a) A typical long intermediate filament complex observed in the SDO/AIA He II 304 Å bandpass on 20-Nov-2011. The arrow points to the location of the *Hinode*/SOT observation in Panel b on the following day. (b) *Hinode*/SOT H α line-center 656.3 nm prominence image on 21-Nov-2011. Note the short horizontal dip segments comprising the majority of the structure.

studied in intermediate prominence sheets, showing evidence of transverse magnetosonic wave propagation with power spectrum peaks at 200–300 s (Schmieder *et al.* 2013).

Intermediate filaments exhibit the same activation events as AR structures but with lower frequency. Intermediate filament eruptions typically involve only individual segments with neighboring segments often remaining unaffected. Su and Van Ballegoijen (2012) model the magnetic field configuration of a large erupting intermediate filament to show that the pre-eruption structure is consistent with that of a magnetic flux rope anchored at one end in an active region that injects destabilizing plasma into the prominence. Recent SDO observations (Schrijver and Title 2011) establish that large intermediate filament eruptions, perhaps themselves triggered by waves generated in AR flares, can trigger nearby filaments to erupt. Török *et al.* (2011) have successfully modeled this cascade of eruptions as an interacting flux rope/arcade field system.

2.3. Quiescent Prominences

Quiescent prominences are typically found in high latitude regions ($>50^\circ$) far from active regions, are generally shorter in latitudinal extent, and associated with weaker photospheric fields. Quiescent prominences are the tallest prominences, sometimes extending 50 Mm or more above the limb. All quiescent prominences have overlying coronal cavities, however the cavity may not be visible in typical EUV filtergrams for some sight angles. Figure 3 shows a typical quiescent prominence extending to about 35 Mm above the photospheric limb.

Typical quiescent prominence structures in visible light passbands are long, predominately quasi-vertical threads. These threads are thicker and more complex than active or intermediate prominence threads and do not appear to me to be structured on horizontally dipped magnetic field lines. Typical thread thickness is 500–700 km in *Hinode*/SOT observations with lengths on the order of 10–20 Mm (Berger *et al.* 2008). However when seen on the disk, quiescent filament threads appear much thinner and more horizontal than limb prominence threads (see e.g., Lin *et al.* 2005). The difference between the on-disk and off-limb appearance of quiescent prominences remains one of the key mysteries in prominence studies. Oscillations in quiescent filament threads have been analyzed by

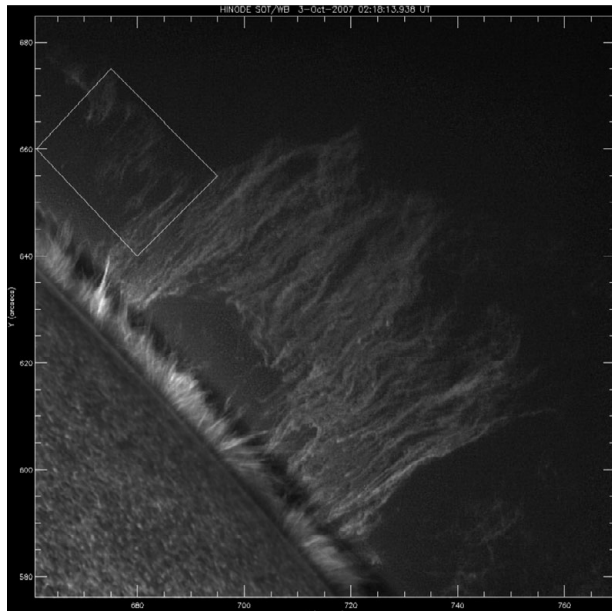


Figure 3. *Hinode/SOT* Ca II 396.8 nm image of a quiescent prominence on the NE limb on 03-October-2007. The box on the left outlines a region of prominence formation with droplet downflows (Haerendel and Berger 2011). The large gap in the lower region of the prominence demarcates the location of an earlier prominence bubble passage. A radial gradient filter is applied to the image causing the dark band above the spicules. Major tickmarks are 20 arcseconds apart.

Ning *et al.* (2009) and Lin *et al.* (2007), showing periods of 200–400 s with a dominant period of 300 s and typical amplitudes of ~ 1000 km.

In EUV passbands, quiescent prominences can exhibit “horn” structures emanating from the top of the prominence (Berger *et al.* 2012; Berger 2012; Vourlidis *et al.* 2012; Plunkett *et al.* 2000). These upwardly curved extensions are not seen in visible light images of quiescent prominences and may represent channels of hot plasma comprising the “prominence corona transition region” (PCTR, Parenti and Vial 2007) connecting the chromospheric prominence to the hotter (Reeves *et al.* 2012) overlying coronal cavity flux rope. In eruptions of quiescent prominences these horns appear to conform exactly to the bottom contour of the rising cavity portion of the flux rope (Régnier *et al.* 2011).

Quiescent prominences are dominated by plasma downflows in the quasi-vertical threads with speeds on the order of 10 km s^{-1} (Schmieder *et al.* 2010; Berger *et al.* 2008). In some cases, isolated “knots” or droplets of plasma are observed to be ejected from quiescent prominences and to fall at near free-fall speeds of $\sim 100 \text{ km s}^{-1}$ (Haerendel and Berger 2011; Hillier *et al.* 2012b). Recent observations have also revealed the “prominence bubble” phenomenon to be common in quiescent prominences (Dudík *et al.* 2012; Hillier *et al.* 2011; Schmieder *et al.* 2010; Berger *et al.* 2010; Ryutova *et al.* 2010; de Toma *et al.* 2008; Berger *et al.* 2008). Prominence bubbles have not yet been identified in intermediate or AR prominences. We defer further discussion of these dynamics to Sec. 3.

2.4. Funnel Prominences

Continuous, full-Sun, multi-spectral, data from SDO/AIA have made it clear that condensation events resulting in “chromospheric” plasma in the corona are common. Prominences and coronal rain are well-known examples, but another type of event has recently

been termed “funnel prominences” (Liu 2013). These events initiate at shallow dips in long coronal loop systems and are usually first detected in the He II 304 Å bandpass as they form into large drainage flows within hours of first nucleation. Superficially, funnel flows resemble quiescent prominences but they can appear at lower latitudes and have not yet been identified with PIL/filament channel systems. Figure 1 of Liu (2013) shows an SDO/AIA composite image that distinguishes between established prominence types and funnel events.

It has been suggested that funnel prominences are equivalent to “cloud prominences” described in earlier ground-based observations (Allen *et al.* 1998), but the latter appear closer in character to “coronal rain” events with high-altitude condensations subsequently flowing at high speeds along coronal loop field lines (Antolin and Verwichte 2011; Schrijver 2001). In contrast, funnel prominence downflows are constrained to narrow conical regions (hence the name) with the plasma apparently flowing *across* coronal magnetic loops. Funnel flow speeds are thus slower than coronal rain speeds, typically only about 30 km s^{-1} . However this is still 2–3 times the typical flow speed in quiescent prominence downflows.

2.5. Prominence pillars and solar “tornados”

Recent SDO/AIA observations in the EUV show apparent rotational motion in so-called prominence “pillars”. Pillars appear as narrow absorption features in the EUV, extending more or less vertically at semi-regular intervals along a filament. They are visible in emission in visible lines as well, but are usually wider than the associated EUV structures. Earlier observations (Pettit 1932) suggest vertical axis rotational motions in prominences, but the continuous full-Sun SDO observations establish these pillars as ubiquitous features of intermediate and quiescent prominences on the Sun†. Figure 4 shows the typical appearance of these structures in a variety of spectral bandpasses.

The apparent rotation of a predominately vertical structure has resulted in these structures being termed “solar tornados” (Su *et al.* 2012). However measurement of continual rotation in these structures is not yet definitive. Several analyses rely solely on AIA movies showing sinusoidal patterns in “time slices” through the structures and such patterns could conceivably be caused by rapid transverse oscillations or counterstreaming flows rather than rotation. However ground-based observations of pillars utilizing doppler velocity measurements show red and blue shifts of $\sim 6 \text{ km s}^{-1}$ (Orozco Suárez *et al.* 2012) to $\sim 20 \text{ km s}^{-1}$ (Wedemeyer-Böhm *et al.* 2013; Schmieder *et al.* 1991) on alternate sides of the pillar, consistent with a rotational motion of the structure. Wedemeyer-Böhm *et al.* (2013) discuss the possible link between this apparent rotation and vortical motions in the photosphere and lower chromosphere (Wedemeyer-Böhm *et al.* 2012; Zhang and Liu 2011; Brandt *et al.* 1988).

The relation of these possibly rotating prominence pillars to filament barbs is unclear (see however recent observations of Li and Zhang (2013)). High resolution images of filament barbs (e.g., Fig. 1 in Lin *et al.* 2005) do not appear anything like the pillars seen in EUV images, with no evidence of rotational motion in the accompanying movies. The detailed relation of solar “tornados” to other prominence structures such as barbs and spines remains to be determined. Also, whether there is a consistent plasma flow *along* the pillars, either upwards or downwards, is unknown. Finally, the term “tornado” has recently also been used to describe large scale rotational flow in a coronal cavity

† To my knowledge, pillars and the tornado phenomenon have not yet been identified in AR prominences.

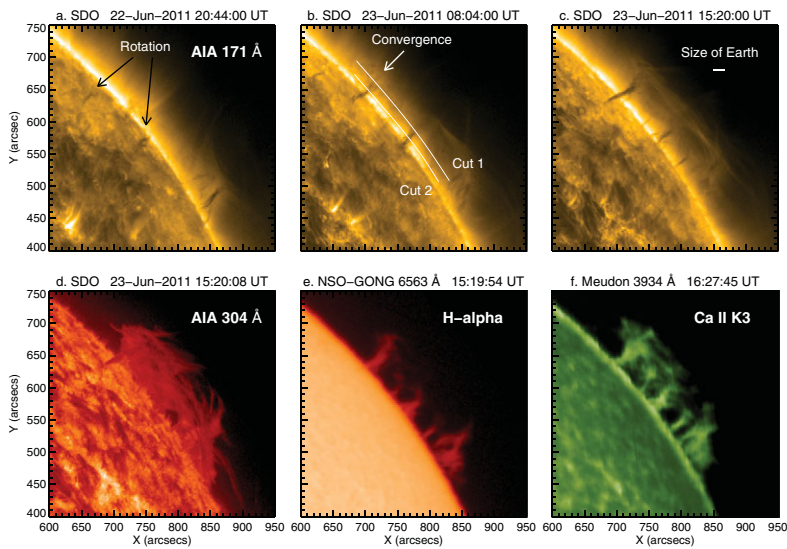


Figure 4. Multispectral view of solar tornadoes from Su *et al.* (2012). The prominence is a large intermediate complex that extends around the limb. Note that the dark apparently rotating pillars in the SDO/AIA EUV bandpasses are significantly narrower than the structures seen in the visible $H\alpha$ and Ca II K-line images. The pillars fan out into the spine region of the prominence at high altitudes to give the appearance of plasma “trees” in the corona.

(Panesar *et al.* 2013), but this is likely distinct from the pillar tornadoes, perhaps related to spinning motions reported by Wang and Stenborg (2010).

3. Quiescent Prominence Fine Structure and Dynamics

We concentrate now on recent findings on quiescent prominences, with an obvious bias towards my own research and interpretations in this area. Quiescent prominences have the advantage over intermediate and AR types of relative freedom from interference by surrounding active region structures, although they have weaker surface field strengths that can make connections to the lower atmosphere less clear. For example, the three-part structure of CMEs consisting of the prominence, coronal cavity, and overlying streamer fields is best seen in polar crown CMEs (Low and Hundhausen 1995; Low 2001). Engvold (1998) and Zirker (1989) give earlier reviews of quiescent prominences. Priest (1989) presents a summary of knowledge to the late-1980s on these objects.

3.1. Formation and downflow dynamics

Mechanisms of prominence formation typically discussed are (1) direct injection of chromospheric plasma into the corona via siphon flows (Pikel’Ner 1971; Engvold and Jensen 1977), magnetic reconnection jets (Litvinenko and Martin 1999; Wang 1999), or flux emergence (Hu and Liu 2000; Okamoto *et al.* 2009); (2) condensation of coronal plasma injected at the footpoints of prominence magnetic field lines (so-called “thermal non-equilibrium” formation) (Xia *et al.* 2012; Luna *et al.* 2012; Karpen and Antiochos 2008; Antiochos and Klimchuk 1991); and (3) direct, or *in situ*, condensation of coronal plasma.

Saito and Tandberg-Hanssen (1973) argue against *in situ* condensation on the grounds that typical prominence densities imply the entire corona contains insufficient mass for the number of observed prominences. However Schmieder *et al.* (1984), following on the suggestions of Malherbe *et al.* (1983), suggest that if the process is dynamic, i.e., if the corona is continually resupplied with plasma, then *in situ* condensation would be possible.

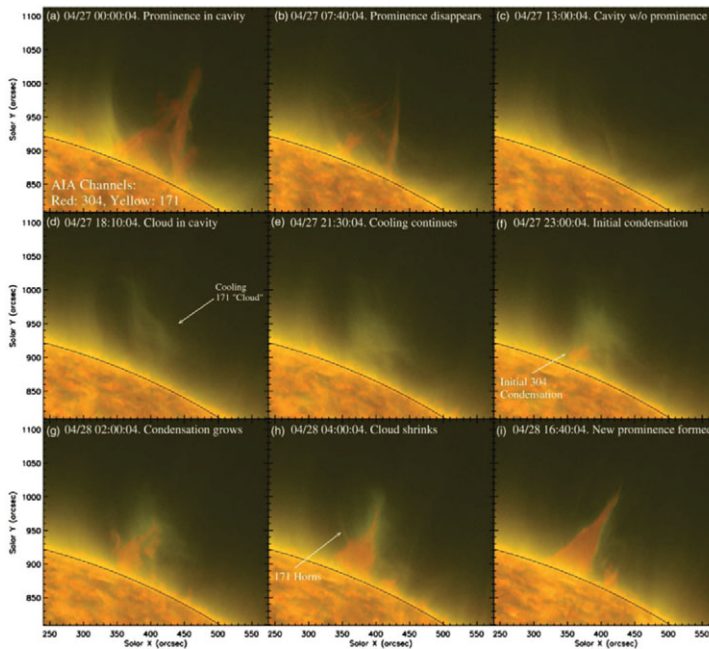


Figure 5. *In situ* condensation of a polar crown quiescent prominence in a coronal cavity from Berger *et al.* (2012). Emission in the $\sim 10^6$ K bandpass dominated by Fe IX 171 Å; chromospheric He II 304 Å emission is shown in orange. Time advances from left to right, top to bottom. The upper right frame shows the empty coronal cavity following the drainage disappearance of the prominence; the lower right shows the prominence fully reformed approximately 27 hours later. The time from first appearance of the hot cloud in the cavity to first evidence of prominence condensation is approximately 5 hours.

Liu *et al.* (2012) observe an intermediate prominence formation via condensation but it is unclear whether it is an *in situ* or a transport condensation event. However Berger *et al.* (2012) analyze multi-wavelength SDO/AIA observations of a coronal cavity and find clear evidence of quiescent prominence formation via *in situ* condensation with no evidence of flows of hot plasma as would be implied by thermal non-equilibrium models. Figure 5 shows a series of SDO/AIA images of the event including the initial disappearance of the prominence due to drainage from the coronal cavity.

Quiescent prominence formation via *in situ* condensation results in vertical drainage of plasma across the apparently horizontal magnetic field lines of the system. For fully ionized plasma such cross-field transport is prevented by Lorentz forces. Low *et al.* (2012a,b) address the physics of cross-field transport of partially ionized prominence plasma. Using analytic radiative cooling functions, they show that a thermal instability can set in that condenses plasma to much lower ionization states and significantly higher densities than typically assumed values (Hirayama 1985). This mechanism is an evolution of the “dragging reconnection” downflows discussed in Low and Petrie (2005) and cited by Chae *et al.* (2008) in his observational study of *Hinode*/SOT prominence downflows. Gilbert *et al.* (2007) also present evidence of cross-field diffusion of neutral He in intermediate prominences, following on initial work by Mercier and Heyvaerts (1977).

Haerendel and Berger (2011) empirically model “magnetic droplet” formation that also allows cross-field transport of condensed prominence plasma. Hillier *et al.* (2012b) analyze *Hinode*/SOT observations and a numerical prominence model to show that reconnection can produce such detached “droplets”, falling at nearly free-fall velocities.

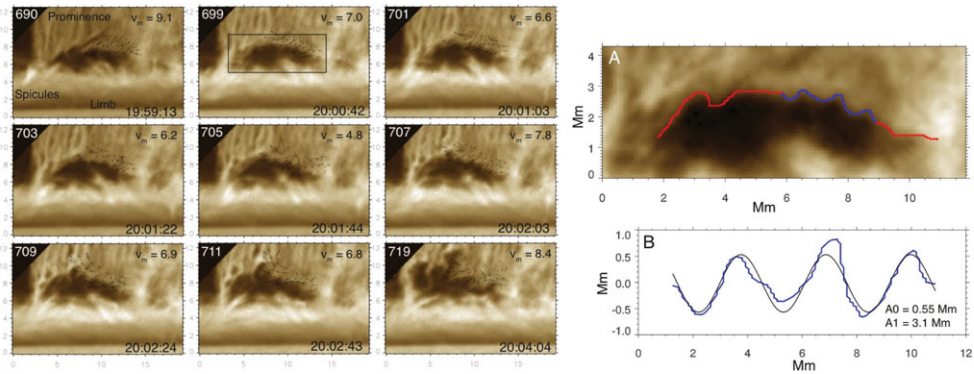


Figure 6. Left: sequence of images in the *Hinode*/SOT $H\alpha$ bandpass showing the development of the RT instability in a prominence bubble. Arrows show the plasma flow as derived by the NAVE code (courtesy of J. Chae). The box in Frame 699 shows the region enlarged on the right. Right: enlargement of the prominence bubble just prior to RT instability onset. The red curve traces the boundary and the blue segment is fit below with a sine function to show perturbations of approximately 3 Mm in wavelength.

Finally Leonardis *et al.* (2012) analyze *Hinode*/SOT time series observations of a quiescent prominence to show that the flow character is consistent with a turbulent cascade, in support of mechanisms that imply a tangled/chaotic magnetic field in quiescent prominence downflows (van Ballegooijen and Cranmer 2010).

3.2. Quiescent prominence bubbles

Prominence bubbles are large ~ 10 Mm, dark (in visible light images) cavities rising into quiescent prominences from below. Bubbles sometimes stagnate at heights of 5–10 Mm before going unstable to form either a single large plume or a series of smaller ones. The plumes are apparently turbulent flows in the bright prominence body that rise with typical speeds of $10\text{--}30\text{ km s}^{-1}$ (Berger *et al.* 2010, 2008), with a horizontal component to the velocity as well (Berger *et al.* 2011; Schmieder *et al.* 2010). Smaller plumes may rise only 10 Mm or so to “fade” into the prominence body while larger plumes may pass entirely through the prominence.

Quiescent prominence bubbles were first observed by Stellmacher and Wiehr (1973). In hindsight, many quiescent prominence images show evidence of bubbles, but single images cannot reveal the dynamics. Following the launch of the *Hinode*/SOT instrument, the phenomenon was rediscovered. Simultaneously, de Toma *et al.* (2008) observed the phenomenon in Mauna Loa Solar Observatory (MLSO) $H\alpha$ patrol images. Ryutova *et al.* (2010) first suggested that the flows are consistent with a Rayleigh-Taylor (RT) buoyancy instability, implying that the bubbles are underdense relative to the prominence.

The RT instability occurs at the interface of fluids of disparate densities in an accelerated frame, typically a static gravitational one. Analysis of prominence bubbles shows that plasma flows *along* the boundary of the bubble can develop Kelvin-Helmholtz (KH) instabilities to form waves that act as the initial perturbations for the RT instability onset (Berger *et al.*, in preparation). Figure 6 shows a local correlation tracking analysis of flows along the boundary of a small quiescent prominence bubble. Note that there is a significant component of the flow upwards and to the left, along the bubble boundary, in the plane of the sky. This lateral flow generates waves on the “upwind” side of the boundary that subsequently grow into the RT instability plumes. This is perhaps the first observation of triggering of the RT instability via KH waves in an astrophysical setting.

Three-dimensional MHD simulations based on the KS prominence model (Kippenhahn and Schlüter 1957) verify that the observed flows are consistent with a magnetic RT

“interchange” instability triggered by the presence of a hot, under-dense, region introduced within the cooler prominence plasma (Hillier *et al.* 2011). This simulation was criticized on the grounds that the perpendicular magnetic field of the KS model is in apparent contradiction to measurements (e.g. Bommier *et al.* 1994) of so-called “guide fields” along the prominence axis. Guide fields supposedly suppress the RT instability due to magnetic tension forces resisting small “undular” mode perturbations. In 2-D analytic models, magnetic tension suppresses all perturbation components parallel to the magnetic field below a critical wavelength given by $\lambda_c = B^2 \cos^2 \theta / g \mu_0 (\rho_2 - \rho_1)$ where B is the prominence magnetic flux density, θ is the angle between the magnetic field and the perturbation wave vector, ρ_2 and ρ_1 are the higher and lower density values of the superposed fluids, respectively, and g is the acceleration of gravity (Chandrasekhar 1981). Assuming $B = 10^{-3}$ Tesla and $\theta \sim 30$ deg as implied by measurements, $\rho_2 = 10^{-9} \text{ kg m}^{-3} \gg \rho_1$ and $g_\odot = 274 \text{ ms}^{-2}$, the critical wavelength is ~ 5 Mm, significantly larger than the perturbations shown in Fig. 6 that develop into plumes.

This discrepancy shows that the simple 2-D magnetic tension analysis does not apply to real prominences which are complex, 3-D, partially ionized systems. Hillier *et al.* (2012a) modifies the KS model to include a guide field and shows that the instability is indeed not suppressed, but that the resulting plumes are larger and less turbulent. Khomenko (2013) studies the effects of partial ionization on the magnetized RT instability to show that the critical wavelength approaches zero as ionization decreases. While issues of line-tying boundary conditions may effect the model outputs, the general conclusion I draw is that in a real 3-D system the magnetic field can only effect certain perturbation modes for any given geometry and there will always arise other perturbations (e.g. those perpendicular to the local field direction) that cannot be suppressed (see, e.g., Stone and Gardiner 2007, who show 3-D MHD simulations of multi-mode RT instabilities.).

The buoyancy of prominence bubbles begs the question of their internal composition. Since they are always dark in H α and Ca II images, the bubbles must either contain plasma heated above the ionization temperatures of these lines ($\sim 138,000$ K for Ca II) or they must be empty voids that allow the background corona to “shine through”. In the latter case, the buoyancy is strictly magnetic; in the former, it could be both magnetic and thermal. Dudík *et al.* (2012) analyze a single bubble and compare SDO/AIA Fe XII 193 Å interior intensity to the surrounding corona. By defining the reference coronal intensity outside of the prominence cavity complex, they show that the bubble interior intensity is less than this background, implying that the bubble is either empty or contains traces of absorbing cooler plasma. Low-resolution spectroscopic studies of prominences apparently support this finding, but these studies have not demonstrated clear discrimination of bubble events in their data (Berlicki *et al.* 2011; Labrosse *et al.* 2011). However, Berger *et al.* (2011) analyze SDO/AIA data to find relative emission (thus implying a hotter-than-background plasma) in two separate events viewed in the 171 Å passband, shown by Parenti *et al.* (2012) to be due to temperatures of at least $\log T = 5.6$ K. In the second event analyzed by Berger *et al.* (2011), the bubble is very large and there is no foreground confusion, nor is there any “prominence” plasma that could lead to PCTR emission in the bubble. Figure 7 confirms that background reference choice is critical to determining the outcome of photometric comparisons: by choosing a nearby background rather than the distant one in Dudík *et al.* (2012), the comparison shows no relative difference in emission, thus implying only that the bubble interior plasma is not *hotter* than the background plasma emission in the Fe XII 193 Å bandpass.

The lower panels of Fig. 7 show a preliminary differential emission measure (DEM) analysis of one of the prominence bubbles and the nearby background corona from Berger *et al.* (2011). Using all six SDO/AIA EUV bandpasses, the DEM analysis implies that

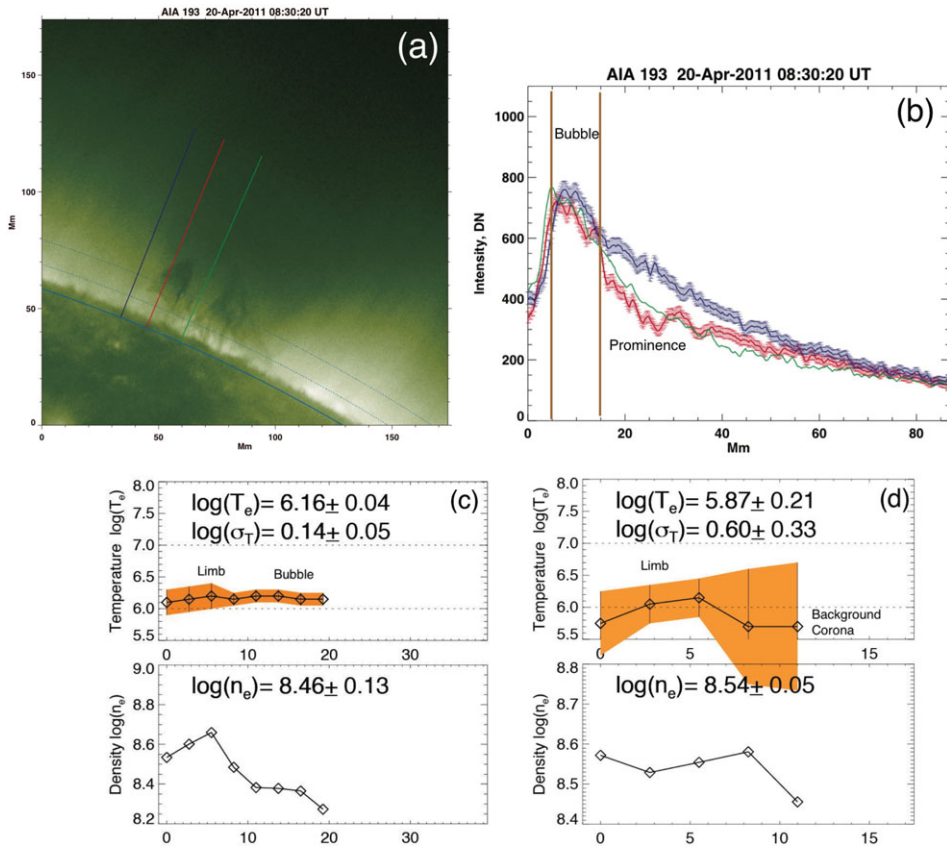


Figure 7. (a) Prominence bubble event on 20-Apr-2011 analyzed in Dudík *et al.* (2012). Colored vertical lines show photometric measurements of the background corona (blue), the bubble (red), and the coronal cavity central region (green). (b) Plots of SDO/AIA intensity in the 193 Å bandpass along the cuts shown in (a). Error bars are $\pm 1\sigma$ deviations due to Poisson statistics. The bubble is indistinguishable from the background in this EUV bandpass. (c) DEM analysis of a prominence bubble from 22-Jun-2010. The top frame show temperature as a function of altitude in Mm from the solar limb; the bottom panel shows density. Limb brightening emission accounts for the first 5–7 Mm of the measurement. (d) Same DEM analysis as in (c) applied to a background coronal region near the prominence. The DEM results show that the bubble is both hotter and lower in density than the background corona. Courtesy M. Aschwanden, LMSAL.

the prominence bubble is both hotter and lower in density than the nearby background plasma, even though the intensity in the bubble in both the Fe XII 193 Å and Fe XIV 211 Å bandpasses is not above background. This analysis supports the conclusion of Berger *et al.* (2011) that prominence bubbles could contain plasma with temperatures up to 10^6 K. While line-of-sight integration is still an issue with DEM analyses of prominences at the limb, it avoids the selectivity biases of photometric comparisons.

4. Conclusion

Although the variation in prominence appearance and dynamics is large, we propose that all prominences can be understood as the partially ionized plasma signatures of coherent magnetic flux ropes in the solar corona. The distinct morphologies of AR, intermediate, and quiescent prominences may thus be due to the relative magnetic field strengths in the associated flux ropes. AR flux ropes are apparently compact 5–10 Mm

structures with field strengths in the kilogauss range, while intermediate flux ropes extend to heights of 20–30 Mm with field strengths of 10–100 gauss, and quiescent polar crown flux ropes extend to heights of 50 Mm or more and have field strengths of 5–10 gauss. It follows that AR prominences are compact horizontal structures with highly constrained flows on long narrow threads forming directly in the core of the flux rope, while intermediate prominences are larger structures with plasma concentrated on shorter horizontal dips in the field (indicating formation in the lower region of the flux rope), and quiescent prominences are extended structures with mostly vertical flows suggesting formation below the flux rope in a current sheet region. Quiescent prominence “horns” also imply that these prominences form below the concave lower portion of the flux rope that manifests in the EUV as a coronal cavity (Gibson 2013; Gibson *et al.* 2004).

This suggests that differences in prominence structure and dynamics can be understood as plasma- β variations in the associated magnetic flux ropes, with quiescent prominences exhibiting possible high- β flow characteristics. Although the suggestion of relatively high- β plasma in any coronal structure is controversial, we point out that *Hinode*/SOT movies of quiescent prominences consistently show flows that appear more “hydrodynamic” in character, as supported by analysis of quiescent prominence plume bow-waves implying plasma- β values of ~ 1 or larger (Hillier 2013; Hillier *et al.* 2012c).

The association of prominences with magnetic flux ropes explains observed characteristics such as spiral and doppler flows in coronal cavities (Panesar *et al.* 2013; Bak Stešlicka *et al.* 2013; Schmit *et al.* 2009), capture and subsequent condensation of coronal plasma in complex field topologies, and energy storage and eruption of the entire flux rope/prominence system due to accumulation of magnetic flux and helicity (Roussev *et al.* 2012; Fan and Gibson 2007; Zhang *et al.* 2006; Gibson and Low 1998). The finding that prominence bubbles may be caused by magnetic flux emergence across the PIL, as modeled by Dudík *et al.* (2012), and that they may contain hot plasma, implies a mechanism for transport of plasma, magnetic flux, and helicity via the Rayleigh-Taylor instability into the overlying flux rope. One can then envision a form of convection in the outer solar atmosphere with hot plasma transported upward and prominences representing the condensation return flow of the system. Similar cyclic/convective processes have been proposed for the quiet Sun (McIntosh *et al.* 2012; Antolin and Rouppe van der Voort 2012; Marsch *et al.* 2008) and coronal rain (Landi *et al.* 2009; Schrijver 2001).

Quoted in the frontispiece of Prof. Tandberg-Hanssen’s book, Secchi (1877) astutely states that “Protruberances [prominences] present all the bizarre and capricious aspects that are absolutely impossible to describe with any exactitude”. We agree and hope that this brief review and personal viewpoint has managed to convey some of the capricious aspects of prominences to yet another generation of solar researchers who will go on to make even more bizarre discoveries about these fascinating objects.

Acknowledgements

We thank the referees for helpful comments and suggestions to improve this review. Dr. Berger was supported by the National Solar Observatory which is operated by the Association of Universities for Research in Astronomy, Inc. (AURA) for the National Science Foundation. *Hinode* is a Japanese mission developed and launched by ISAS/JAXA, collaborating with NAOJ as a domestic partner, NASA (US) and STFC (UK) as international partners. Support for the post-launch operation is provided by JAXA and NAOJ (Japan), STFC (UK), NASA, ESA, and NSC (Norway). SDO/AIA data are available to the public without restriction.

References

- Ahn, K., Chae, J., Cao, W., & Goode, P. R.: 2010, *ApJ* **721**, 74
- Allen, U. A., Bagenal, F., & Hundhausen, A. J.: 1998, in *New Perspectives on Solar Prominences*, IAU Colloquium 167, D. F. Webb, D. M. Rust, and B. Schmieder (eds.), *Astron. Soc. of the Pacific Conf. Series* **150**, p. 290
- Antiochos, S. K. & Klimchuk, J. A.: 1991, *ApJ* **378**, 372
- Antolin, P. & Rouppe van der Voort, L.: 2012, *ApJ* **745**, 152
- Antolin, P. & Verwichte, E.: 2011, *ApJ* **736**, 121
- Aulanier, G. & Demoulin, P.: 1998, *A & A* **329**, 1125
- Aulanier, G., Demoulin, P., van Driel-Gesztelyi, L., *et al.*: 1998, *A & A* **335**, 309
- Bak Stešlicka, U., Gibson, S. E., Fan, Y., *et al.*: 2013, *ApJ* **770**, L28
- Ballester, J. L.: 2006, *Space Sci Rev* **122**, 129
- Berger, T.: 2012, in *The Second ATST-EAST Meeting: Magnetic Fields from the Photosphere to the Corona*, T. Rimmele, A. Tritschler, F. Woeger, *et al.* (eds.), *Astron. Soc. of the Pacific Conf. Series* **463**, p. 147
- Berger, T. E., Liu, W., & Low, B. C.: 2012, *ApJ* **758**, L37
- Berger, T., Testa, P., Hillier, *et al.*: 2011, *Nature* **472**, 197
- Berger, T. E., Slater, G., Hurlburt, *et al.*: 2010, *ApJ* **716**, 1288
- Berger, T. E., Shine, R. A., Slater, G. L., *et al.*: 2008, *ApJ* **676**, L89
- Berlicki, A., Gunár, S., Heinzel, P., Schmieder, B., & Schwartz, P.: 2011, *A & A* **530**, A143
- Bocchialini, K., Baudin, F., Koutchmy, S., Pouget, G., & Solomon, J.: 2011, *A & A* **533**, 96
- Bommier, V., Landi Degl'Innocenti, E. *et al.*: 1994, *Sol Phys* **154**, 231
- Brandt, P. N., Scharmer, G. B., Ferguson, S. *et al.*: 1988, *Nature* **335**, 238
- Casini, R., López Ariste, A., Tomczyk, S., & Lites, B. W.: 2003, *ApJ* **598**, L67
- Chae, J., Ahn, K., Lim, E.-K., Choe, G. S., & Sakurai, T.: 2008, *ApJ* **689**, L73
- Chandrasekhar, S.: 1981, *Hydrodynamic and hydromagnetic stability*, Dover, 3rd edition
- de Toma, G., Casini, R., Burkpile, J. T., & Low, B. C.: 2008, *ApJ* **687**, L123
- Demoulin, P., Malherbe, J. M., Schmieder, B., & Raadu, M. A.: 1987, *A & A* **183**, 142
- Dudík, J., Aulanier, G., Schmieder, B., & Bommier, V.; Roudier, T.: 2008, *Sol Phys* **248**, 29
- Dudík, J., Aulanier, G., Schmieder, B., Zapiór, M., & Heinzel, P.: 2012, *ApJ* **761**, 9
- Engvold, O.: 1998, in *New Perspectives on Solar Prominences*, IAU Coll. 167, D. F. Webb, D. M. Rust, and B. Schmieder (eds.), *Astron. Soc. of the Pacific Conf. Series* **150**
- Engvold, O. & Jensen, E.: 1977, *Sol. Phys.* **52**, 37
- Fan, Y. & Gibson, S. E.: 2007, *ApJ* **668**, 1232
- Filippov, B. & Koutchmy, S.: 2002, *Sol. Phys.* **208**, 283
- Gaizauskas, V., Zirker, J. B., Sweetland, C., & Kovacs, A.: 1997, *ApJ* **479**, 448
- Gibson, S.: 2013, in these proceedings
- Gibson, S. E., Fan, Y., Mandrini, C., Fisher, G., & Demoulin, P.: 2004, *ApJ* **617**, 600
- Gibson, S. & Low, B.: 1998, *ApJ* **493**, 460
- Gilbert, H., Kilper, G., & Alexander, D.: 2007, *ApJ* **671**, 978
- Gunár, S.: 2013, in these proceedings
- Haerendel, G. & Berger, T.: 2011, *ApJ* **731**, 82
- Heinzel, P., Schmieder, B., Fárnik, F., Schwartz, P., *et al.*: 2008, *ApJ* **686**, 1383
- Hillier, A.: 2013, in these proceedings
- Hillier, A., Hillier, R., & Tripathy, D.: 2012c, *ApJ* **761**, 106
- Hillier, A., Isobe, H., Shibata, K., & Berger, T.: 2012b, *ApJ* **756**, 110
- Hillier, A., Berger, T., Isobe, H., & Shibata, K.: 2012a, *ApJ* **746**, 120
- Hillier, A., Isobe, H., Shibata, K., & Berger, T.: 2011, *ApJ* **736**, L1
- Hirayama, T.: 1985, *Sol. Phys.* **100**, 415
- Hu, Y. Q. & Liu, W.: 2000, *ApJ* **540**, 1119
- Karpen, J. T. & Antiochos, S. K.: 2008, *ApJ* **676**, 658
- Kippenhahn, R. & Schlüter, A.: 1957, *Zeitschrift für Astrophysik* **43**, 36
- Khomenko, E.: 2013, in these proceedings
- Kucera, T., Tovar, M., & de Pontieu, B.: 2003, *Sol. Phys.* **212**, 81

- Kuckein, C., Martinez Pillet, V., & Centeno, R.: 2012, *A & A* **542**, A112
- Labrosse, N., Schmieder, B., Heinzl, P., & Watanabe, T.: 2011, *A&A* **531**, 69
- Labrosse, N., Heinzl, P., Vial, J. C., *et al.*: 2010, *Space Sci Rev* **151**, 243
- Landi, E., Miralles, M. P., Curdt, W., & Hara, H.: 2009, *ApJ* **695**, 221
- Lemen, J. R., Title, A. M., Akin, *et al.*: 2011, *Sol. Phys.* **275**, 17
- Leonardis, E., Chapman, S. C., & Foullon, C.: 2012, *ApJ* **745**, 185
- Li, T. & Zhang, J.: 2013, *ApJ* **770**, L25
- Lin, Y., Engvold, O., Rouppe Van Der Voort, L. H. M., *et al.*: 2007, *Sol. Phys.* **246**, 65
- Lin, Y., Engvold, O., Van Der Voort, L. H. M., *et al.*: 2005, *Sol. Phys.* **226**, 239
- Lites, B. W., Kubo, M., Berger, T., *et al.*: 2010, *ApJ* **718**, 474
- Litvinenko, Y. E. & Martin, S. F.: 1999, *Sol. Phys.* **190**, 45
- Liu, W.: 2013, these proceedings
- Liu, W., Berger, T. E., & Low, B. C.: 2012, *ApJ* **745**, L21
- López Ariste, A. & Casini, R.: 2003, *ApJ* **582**, L51
- Low, B.: 2001, *J. Geophys. Res.* **106**, 25
- Low, B. C., Berger, T., & Casini, R.: 2012a, *ApJ*
- Low, B. C. & Hundhausen, J. R.: 1995, *ApJ* **443**, 818
- Low, B. C., Liu, W., Berger, T., & Casini, R.: 2012b, *ApJ* **757**, 21
- Low, B. C. & Petrie, G. J. D.: 2005, *ApJ* **626**, 551
- Luna, M., Karpen, J. T., & DeVore, C. R.: 2012, *ApJ* **746**, 30
- Mackay, D. H., Gaizauskas, V., & Yeates, A. R.: 2008, *Sol. Phys.* **248**, 51
- Mackay, D. H., Karpen, J. T., Ballester, J. L., *et al.*: 2010, *Space Sci Rev* **151**, 333
- Malherbe, J. M., Priest, E. R., Forbes, T. G., & Heyvaerts, J.: 1983, *A & A* **127**, 153
- Marsch, E., Tian, H., Sun, J., Curdt, W., & Wiegmann, T.: 2008, *ApJ* **685**, 1262
- Martin, S. F.: 1998, *Sol. Phys.* **182**, 107
- Martin, S. F., Lin, Y., & Engvold, O.: 2008, *Sol. Phys.* **250**, 31
- McIntosh, S. W., Tian, H., Sechler, M., & De Pontieu, B.: 2012, *ApJ* **749**(1), 60
- Mercier, C. & Heyvaerts, J.: 1977, *A&A* **61**, 685
- Merenda, L., Bueno, J. T., Degl'Innocenti, E. L., & Collados, M.: 2006, *ApJ* **642**, 554
- Ning, Z., Cao, W., Okamoto, T. J., Ichimoto, K., & Qu, Z. Q.: 2009, *A & A* **499**, 595
- Okamoto, T. J., Tsuneta, S., Berger, T. E., *et al.*: 2007, *Science* **318**, 1577
- Okamoto, T. J., Tsuneta, S., Lites, *et al.*: 2009, *ApJ* **697**, 913
- Orozco Suárez, D., Asensio Ramos, A., & Trujillo Bueno, J.: 2012, *ApJ* **761**, L25
- Panesar, N. K., Innes, D. E., Tiwari, S. K., & Low, B. C.: 2013, *A & A* **549**, A105
- Parenti, S., Schmieder, B., Heinzl, P., & Golub, L.: 2012, *ApJ* **754**(1), 66
- Parenti, S. & Vial, J.-C.: 2007, *A & A* **469**, 1109
- Pettit, E.: 1932, *ApJ* **76**, 9
- Pikel'Ner, S. B.: 1971, *Sol. Phys.* **17**, 44
- Plunkett, S. P., Vourlidis, A., Šimberová, S., *et al.*: 2000, *Sol. Phys.* **194**, 371
- Priest, E. R.: 1989, *Dynamics and Structure of Quiescent Solar Prominences* Kluwer Academic Publishers: Dordrecht
- Reeves, K. K., Gibson, S. E., Kucera, T. A., Hudson, H. S., & Kano, R.: 2012, *ApJ* **746**, 146
- Régnier, S., Walsh, R. W., & Alexander, C. E.: 2011, *A & A* **533**, L1
- Roussev, I. I., Galsgaard, K., Downs, C., *et al.*: 2012, *Nature Physics* **8**, 1
- Ryutova, M., Berger, T., Frank, Z., Tarbell, T., & Title, A.: 2010, *Sol. Phys.* p. 170
- Saito, K. & Tandberg-Hanssen, E.: 1973, *Sol. Phys.* **31**, 105
- Schmieder, B., Kucera, T. A., Knizhnik, K., Luna, M., Lopez-Ariste, A., Toot, D. *ApJ*, **777**, 108
- Schmieder, B., Chandra, R., Berlicki, A., & Mein, P.: 2010, *A & A* **514**, 68
- Schmieder, B., Malherbe, J. M., Mein, P., & Tandberg-Hanssen, E.: 1984, *A & A* **136**, 81
- Schmieder, B., Raadu, M. A., & Wiik, J. E.: 1991, *A & A* **252**, 353
- Schmit, D. J., Gibson, S. E., Tomczyk, S., *et al.*: 2009, *ApJ* **700**, L96
- Schrijver, C. J.: 2001, *Sol. Phys.* **198**, 325
- Schrijver, C. J. & Title, A. M.: 2011, *J. Geophys. Res.* **116**, A04108

- Secchi, A.: 1877 *Le Soleil* Gauthier-Villars: Paris, vols. 1 & 2
- Stellmacher, G. & Wiehr, E.: 1973, *A & A* **24**, 321
- Stone, J. M. & Gardiner, T.: 2007, *Phys. Fluids* **19**, 4104
- Su, Y. & Van Ballegoijen, A.: 2012, *ApJ* **757**, 168
- Su, Y., Wang, T., Veronig, A., Temmer, M., & Gan, W.: 2012, *ApJ* **756**, L41
- Tandberg-Hanssen, E.: 1995, *The Nature of Solar Prominences*, Kluwer Academic: Dordrecht
- Török, T., Panasenco, O., Titov, V. S., *et al.*: 2011, *ApJ* **739**, L63
- Tsuneta, S., Ichimoto, K., Katsukawa, *et al.*: 2008, *Sol. Phys.* **249**, 167
- van Ballegoijen, A. A. & Cranmer, S. R.: 2010, *ApJ* **711**, 164
- Vourlidas, A., Lynch, B. J., Howard, R. A., & Li, Y.: 2012, *Sol. Phys.* **284**, 179
- Wang, H., Chae, J., Gurman, J. B., & Kucera, T. A.: 1998, *Sol Phys* **183**, 91
- Wang, Y.-M.: 1999, *ApJ* **520**, L71
- Wang, Y.-M. & Stenborg, G.: 2010, *ApJ* **719**, L181
- Wedemeyer-Böhm, S., Scullion, E., Rouppe van der Voort, L., *et al.*: 2013, *ApJ* **774**, 123
- Wedemeyer-Böhm, S., Scullion, E., Steiner, O., *et al.*: 2012, *Nature* **486**, 505
- Xia, C., Chen, P. F., & Keppens, R.: 2012, *ApJ* **748**, L26
- Zhang, J. & Liu, Y.: 2011, *ApJ* **741**, L7
- Zhang, M., Flyer, N., & Low, B. C.: 2006, *ApJ* **644**, 575
- Zirker, J. B.: 1989, *Sol. Phys.* **119**, 341
- Zirker, J. B., Engvold, O., & Martin, S. F.: 1998, *Nature* **396**, 440